ORIGINAL ARTICLE

CD146 is a novel marker for highly tumorigenic cells and a potential therapeutic target in malignant rhabdoid tumor

S Nodomi[1], K Umeda[1], S Saida[1], T Kinehara[1], T Hamabata[1], T Daifu[1], I Kato[1], H Hiramatsu[1], K-i Watanabe[1], Y Kuwahara[2], T Iehara[2], S Adachi[3], E Konishi[4], T Nakahata[5], H Hosoi[2] and T Heike[1]

Malignant rhabdoid tumor (MRT) is a rare, highly aggressive pediatric malignancy that primarily develops during infancy and early childhood. Despite the existing standard of intensive multimodal therapy, the prognosis of patients with MRT is dismal; therefore, a greater understanding of the biology of this disease is required to establish novel therapies. In this study, we identified a highly tumorigenic sub-population in MRT, based on the expression of CD146 (also known as melanoma cell adhesion molecule), a cell adhesion molecule expressed by neural crest cells and various derivatives. CD146+ cells isolated from four MRT cell lines by cell sorting exhibited enhanced self-renewal and invasive potential in vitro. In a xenograft model using immunodeficient NOD/Shi-scid IL-2Rγ-null mice, purified CD146+ cells obtained from MRT cell lines or a primary tumor exhibited the exclusive ability to form tumors in vivo. Blocking of CD146-related mechanisms, either by short hairpin RNA knockdown or treatment with a polyclonal antibody against CD146, effectively suppressed tumor growth of MRT cells both in vitro and in vivo via induction of apoptosis by inactivating Akt. Furthermore, CD146 positivity in immunohistological analysis of 11 MRT patient samples was associated with poor patient outcomes. These results suggest that CD146 defines a distinct sub-population in MRT with high tumorigenic capacity and that this marker represents a promising therapeutic target.

INTRODUCTION

Malignant rhabdoid tumor (MRT) is a rare and highly aggressive tumor that primarily develops in infancy and early childhood.[1,2] Malignant rhabdoid tumor of the kidney (MRTK) constitutes 1.8% of pediatric renal tumors,[3] whereas MRT in the central nervous system, referred to as atypical teratoid rhabdoid tumor (ATRT), constitutes 10–20% of central nervous system tumors in children < 3 years old.[4,5] The majority of tumors are characterized by loss-of-function of the SMARCB1/INI1/SNF5/BAF47 tumor-suppressor gene, located on chromosome 22q11.2.[6,7] Despite the existing standard of intensive multimodal therapy, the long-term survival rate of patients with MRT is < 30%; therefore, a greater understanding of the biology of this tumor is necessary for development of more effective treatments.[5,8]

Tumors are composed of heterogeneous cell populations containing a sub-population termed tumor-initiating cells (TICs), which have the capacity to self-renew and differentiate into their progeny.[9–11] Accumulating evidence suggests that TICs exist in acute myeloid leukemia,[12] as well as in several types of solid tumors.[13,14] As TICs are thought to have crucial roles in tumor recurrence after therapy, specific markers for these cells are expected to be promising therapeutic targets.[15] TICs often share many immunophenotypic similarities with normal stem cells of the same origin. Although the origin of MRT has remained unidentified so far, gene expression profiling and immunostaining analysis have raised the possibility that MRT is derived from neural crest, a transient embryonic cell population that gives rise to a wide range of derivatives.[16–18] CD133, a neural or neural crest

stem cell marker, has been used to identify TICs in various types of malignancies.[11] CD133 marks radio-resistant cells in ATRT and a highly tumorigenic sub-population in MRTK;[19,20] however, no therapeutic application targeting CD133 has yet been developed.

CD146 is a cell adhesion molecule belonging to the immunoglobulin superfamily. In adults, expression of CD146 is restricted to a subset of normal cell types, including endothelial cells, ganglion cells and activated T lymphocytes;[21,22] by contrast, it is widely expressed in embryonic tissues, including neural crest and its derivatives.[23] CD146 is involved in various physiological processes, including cell–cell and cell–matrix interactions, cell migration, and signaling, as well as morphogenesis during development.[22] Growing evidence demonstrated that CD146 promotes tumor growth, angiogenesis and metastasis.[22] Furthermore, CD146 expression is strongly associated with adverse clinical outcome of melanoma, a malignancy derived from the neural crest linage.[22] Hence, CD146 is a promising candidate for immunotherapy against melanoma.[24]

We also found that CD146 defined a subset of highly tumorigenic cells in MRT, and our novel anti-CD146 polyclonal antibody and knockdown of CD146 inhibited tumor growth by inducing apoptosis, suggesting that this surface marker is a potential therapeutic target for treatment of MRT.

RESULTS

CD146+ MRT cells possess enhanced self-renewal and invasive potential in vitro

To identify a surface marker to define highly tumorigenic cells in MRT, we first subjected MRT cell lines and primary tumors from

[1]Department of Pediatrics, Graduate School of Medicine, Kyoto University, Kyoto, Japan; [2]Department of Pediatrics, Graduate School of Medical Science, Kyoto Prefectural University of Medicine, Kyoto, Japan; [3]Department of Human Health Sciences, Graduate School of Medicine, Kyoto University, Kyoto, Japan; [4]Department of Surgical Pathology, Graduate School of Medical Science, Kyoto Prefectural University of Medicine, Kyoto, Japan and [5]Department of Clinical Application, Center for iPS Cell Research and Application, Kyoto University, Kyoto, Japan. Correspondence: Dr K Umeda, Department of Pediatrics, Graduate School of Medicine, Kyoto University, 54 Kawahara-cho, Shogoin, Sakyo-ku, Kyoto City, Kyoto 606-8507, Japan.
E-mail: umeume@kuhp.kyoto-u.ac.jp
Received 6 January 2015; revised 10 January 2016; accepted 12 February 2016; published online 4 April 2016

patients with ATRT to flow cytometric analysis to examine the expression of several surface antigens related to neural crest specification and/or differentiation. Expression of CD146 ranged from 13 to 98% in cell lines (Figure 1a), and a small CD146$^+$ cell sub-population was detected in ATRT primary tumors (Figure 1b), whereas CD133-expressing cells were hardly detectable in both cell lines and primary tumors (Figure 1b and Supplementary Table 1). As TICs from various types of malignancies are enriched in sphere culture systems,[25] we compared the expression levels of each surface marker in sphere-forming and adherent cells. As shown in Supplementary Table 1, CD146$^+$ cells were as enriched in sphere-forming cells as CD133$^+$ cells, leading to the hypothesis that CD146 may also be a candidate marker of TICs in MRT.

To test this hypothesis, we evaluated the self-renewal and invasive potential of purified CD146$^+$ cells by sphere-forming and invasion assays, respectively (Supplementary Figure 1A). Both of these potentials are associated with TIC phenotype.[26] The number of spheres was significantly higher in CD146$^+$ cells than in CD146$^-$ cells (Figures 2a and b). CD146$^+$ cells were never detected in spheres derived from CD146$^-$ cells (Supplementary Figure 1B), arguing that sphere formation itself does not induce expression of CD146. When sorted CD146$^+$ cells were attached to cell culture plates, both CD146$^+$ and CD146$^-$ cells were generated during serial passages, and sorted CD146$^-$ cells could also produce CD146$^+$ cells, albeit less efficiently (Supplementary Figure 1C), indicating that CD146$^+$ and CD146$^-$ cells may exhibit reversible phenotypic plasticity under two-dimensional culture conditions.[27] As previous reports suggest that CD133$^+$ cells have characteristics of TICs in MRT,[19,20] we compared the sphere-forming potential of CD133$^+$ cells with that of CD146$^+$ cells in MRT cell lines. In the MP-MRT-AN and KP-MRT-NS cell lines, all CD133$^+$ cells also expressed CD146. In the KP-MRT-RY and KP-MRT-YM cell lines, the number of
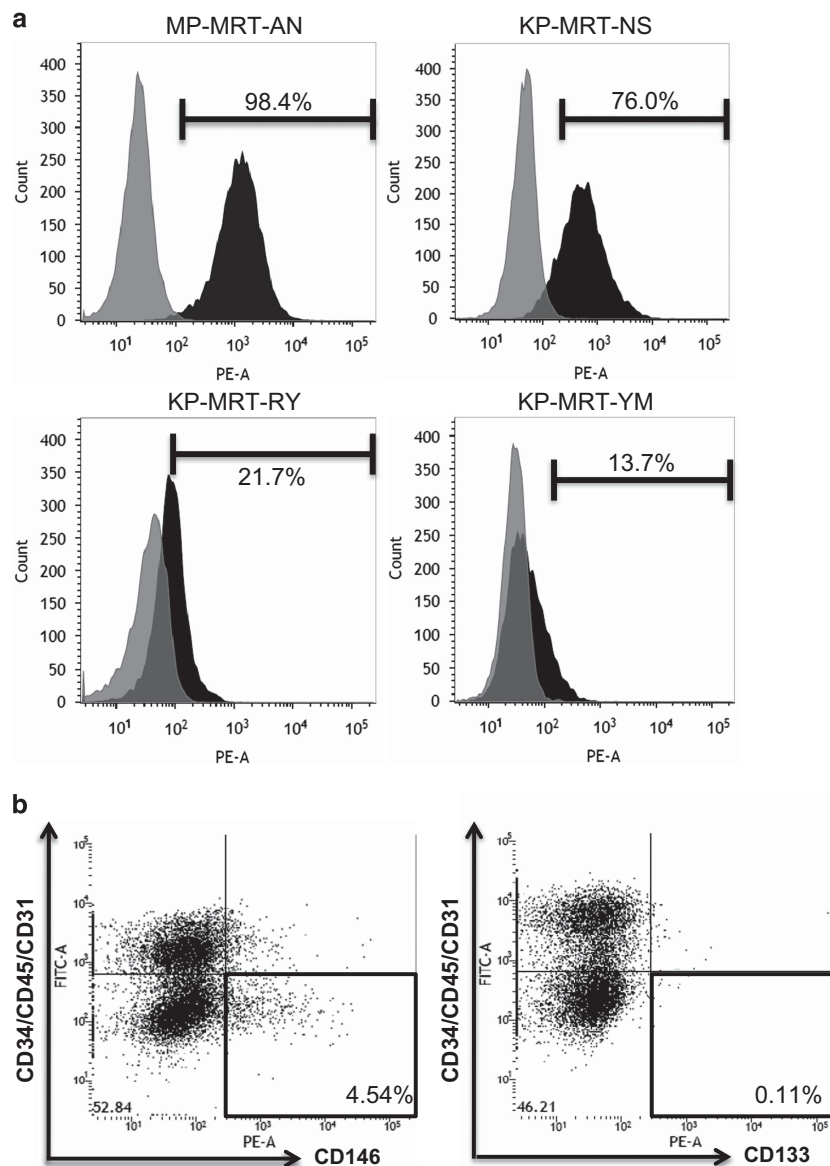

Figure 1. CD146 expression in MRT cell lines and primary tumors. (a) MP-MRT-AN, KP-MRT-NS, KP-MRT-RY and KP-MRT-YM cells were stained with anti-CD146 (black histograms) or isotype-matched control antibodies (gray histograms), and then analyzed by flow cytometry. (b) Representative flow cytometric profile of ATRT primary tumor cells stained with anti-CD146 and anti-CD133 antibodies, showing that a small CD146$^+$ sub-population was present, whereas CD133$^+$ cells were rarely observed.
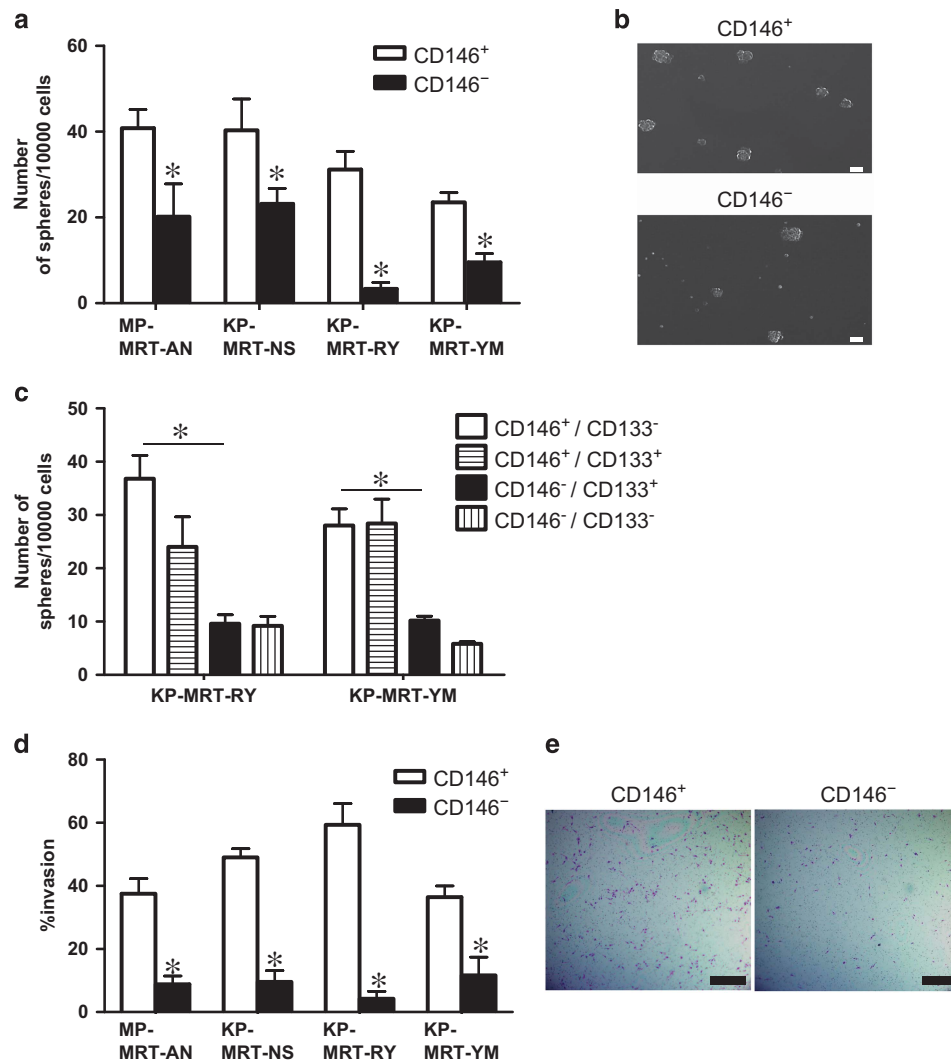
Figure 2. CD146^{+} MRT cells show more enhanced self-renewal and invasive potential than CD146^{−} cells *in vitro*. (**a**) Sphere-forming potential of purified CD146^{+} and CD146^{−} MRT cells. (**b**) Representative light micrographs of spheres generated from CD146^{+} and CD146^{−} KP-MRT-NS cells. Scale bars = 50 µm. (**c**) Sphere-forming potential of purified CD146^{+} and CD133^{+} MRT cells. (**d**) Invasive potential of CD146^{+} and CD146^{−} MRT cells *in vitro*. (**e**) Representative light micrographs of invaded CD146^{+} and CD146^{−} KP-MRT-RY cells (scale bars = 500 µm). Error bars indicate s.d. All experiments were performed in at least triplicate (*$P < 0.05$).

spheres was significantly higher in CD146^{+}/CD133^{−} cells than in CD146^{−}/CD133^{+} cells (Figure 2c). Furthermore, CD146^{+} cells exhibited significantly more invasive behavior *in vitro* than CD146^{−} cells (Figures 2d and e). Collectively, these data demonstrate that CD146^{+} cells exhibited greater enhanced self-renewal and invasive potential than CD146^{−} cells *in vitro*.

CD146^{+} MRT cells initiate tumor formation and replicate tumor heterogeneity *in vivo*
To evaluate *in vivo* tumor formation ability, were subcutaneously injected sorted CD146^{+} and CD146^{−} cells into the flanks of immunodeficient NOG mice. Limiting dilution studies revealed that as few as 1000 CD146^{+} cells were capable of generating tumors 12 weeks after transplantation, whereas CD146^{−} cells did not form tumors even if 10 000 cells were injected (Table 1). The histology of the tumors in NOG mice revealed that tumor cells were round to polygonal, had prominent nucleoli and eosinophilic cytoplasm, and were negative for INI1, similar to the histological findings of MRT (Supplementary Figure 2). To determine which

sub-population was serially transplantable, engrafted tumors were purified into CD146^{+} and CD146^{−} fractions and re-transplanted in NOG mice. As expected, formation of secondary and tertiary tumors, whose morphologies were similar to the primary tumor, was observed only in mice injected with CD146^{+} cells. Exclusive stable engraftment, as well as successful serial engraftment of CD146^{+} cells, was also observed after subcutaneous injection of early passage xenografts of primary ATRT cells (Table 1 and Supplementary Figure 2). Histological analyses revealed monotonous tumor cell proliferation with scattered INI1^{+} blood cells, endothelial cells and stromal cells (Supplementary Figure 2). Notably, flow cytometric analysis demonstrated that the engrafted tumors contained proportions of CD146^{+} and CD146^{−} cells similar to those observed before transplant in at least some cell lines and primary tumors (Figures 3a and b and Supplementary Figure 3), suggesting that CD146^{+} cells regenerate phenotypically and functionally heterogeneous cell populations during *in vivo* tumor formation. Collectively, these data indicate that the expression of CD146 defined highly tumorigenic sub-population in at least some of the MRTs we examined.

Table 1. Tumor formation ability of sorted CD146$^+$ and CD146$^-$ MRT cells in NOG mice

Samples	Cells per injection	Tumors/Injections					
		Primary transplantation		Secondary transplantation		Tertiary transplantation	
		CD146$^+$	CD146$^-$	CD146$^+$	CD146$^-$	CD146$^+$	CD146$^-$
MP-MRT-AN	10 000	5/5*	0/5				
	1000	4/4*	0/4	4/5*	0/6	3/4	ND
	Tumor-initiating frequency (95% CI)	(>1/1557)	(<1/18 026)				
KP-MRT-NS	10 000	5/7*	0/7				
	1000	5/8*	0/8	4/5*	0/6	4/4*	0/4
	Tumor-initiating frequency (95% CI)	1/4115 (1/1812–1/9346)	(<1/26 037)				
KP-MRT-RY	10 000	6/6*	0/6				
	1000	6/6*	0/6	4/4*	0/4	2/4	ND
	Tumor-initiating frequency (95% CI)	(>1/1071)	(<1/22 031)				
KP-MRT-YM	10 000	5/6*	0/6				
	1000	0/6	0/6	5/6*	0/6	3/4	ND
	Tumor-initiating frequency (95% CI)	1/2061 (1/709–1/5990)	(<1/22 031)				
Xenografts of clinical sample (patient #4)	10 000	5/8*	0/8				
	1000	0/4	0/4	2/4	0/6	0/4	0/6
	Tumor-initiating frequency (95% CI)	1/11056 (1/4518–1/27 058)	(<1/28 040)				

Abbreviations: CI, confidence interval; MRT, malignant rhabdoid tumor; ND, not done. In all cases, P-values are calculated comparing tumor formation at different cell dilutions (*P < 0.05).
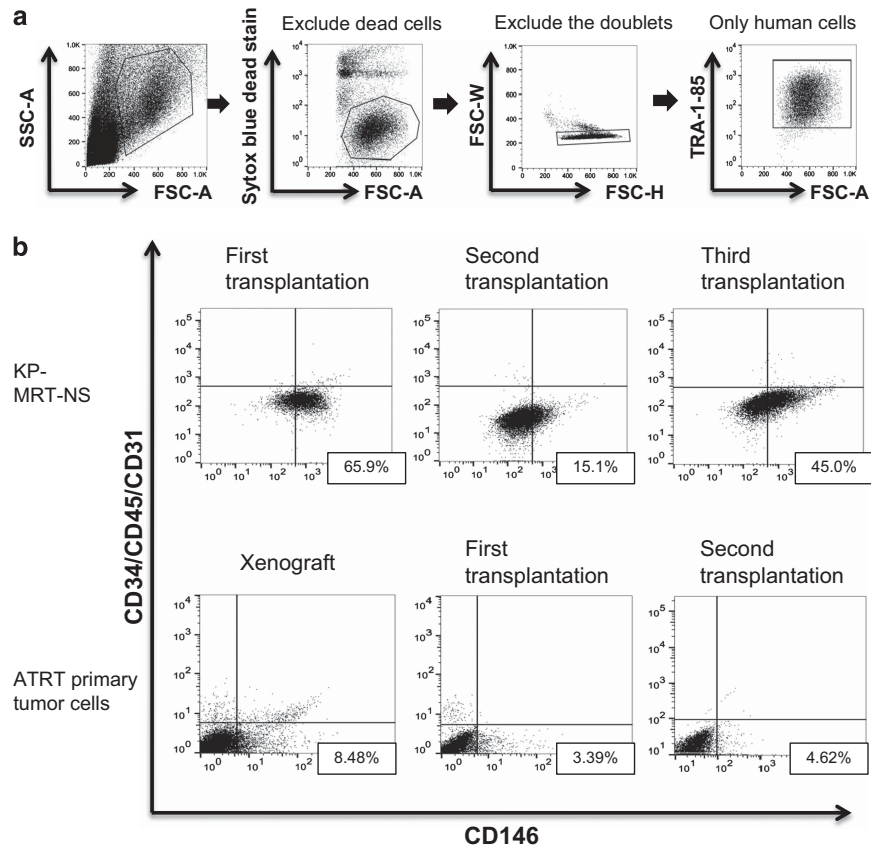

Figure 3. CD146$^+$ cells replicate phenotypically heterogeneous cell populations during in vivo tumor formation. (**a**) Gating strategy for sorting live MRT cells. (**b**) Flow cytometric analysis showing the expression of CD146 in engrafted KP-MRT-NS cells and ATRT primary tumor cells during serial transplantation.
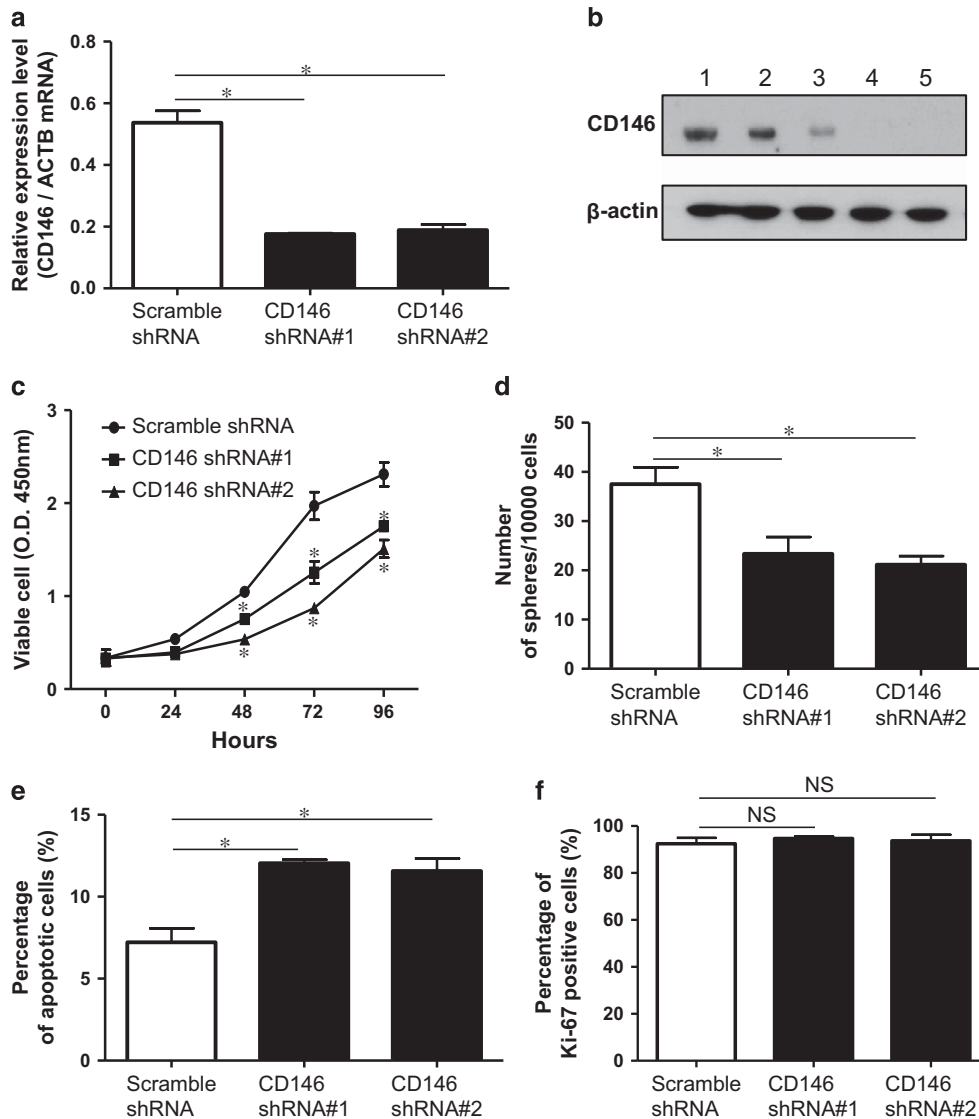
Figure 4. Knockdown of CD146 suppresses self-renewal potential and survival of MRT cells by inducing apoptosis. (a) *CD146* mRNA levels in shRNA-treated KP-MRT-NS cells were analyzed by qRT–PCR. *ACTB* mRNA served as an internal control. (b) Western blotting of CD146 and β-actin after shRNA transduction (lane 1, purified CD146$^+$ KP-MRT-NS cells; lane 2, Scramble shRNA; lane 3, CD146 shRNA#1; lane 4, CD146 shRNA#2; lane 5, purified CD146$^-$ KP-MRT-NS cells). (c) WST-8 assays after transduction of CD146-specific shRNA (closed squares and triangles) or scrambled shRNA (closed circles). OD, optical density. (d) Sphere-forming assays after shRNA transduction. (e) Apoptosis assays after shRNA transduction. (f) Proliferation assays after shRNA transduction. Error bars indicate s.d. All experiments were performed in triplicate (*$P < 0.05$). NS, not significant.

Blocking the CD146-related mechanisms efficiently suppresses survival of MRT cells by inducing apoptosis

To confirm the tumorigenic effect of CD146 in MRT, we used short hairpin RNA (shRNA) to knockdown CD146 in KP-MRT-NS cells. Transfection efficiencies of CD146 shRNA#1, CD146 shRNA#2 and scrambled shRNA were confirmed by quantitative reverse transcription polymerase chain reaction (qRT–PCR) and western blotting (Figures 4a and b). WST-8 and sphere-forming assays demonstrated that knockdown of CD146 significantly reduced survival and self-renewal potential of MRT cells, respectively (Figures 4c and d). Furthermore, apoptosis assays revealed that knockdown of CD146 significantly increased the number of apoptotic cells (Figure 4e). On the other hand, Ki-67 staining revealed that knockdown of CD146 had no effect on cell proliferation (Figure 4f). To eliminate CD146$^+$ MRT cells more effectively, we developed a rabbit polyclonal antibody against CD146 (Supplementary Figures 4A and B). WST-8 assays revealed that anti-CD146 antibody significantly reduced survival of MRT cells in a dose-dependent manner, relative to normal rabbit serum (Figure 5a and Supplementary Figure 5A). By contrast, this antibody did not reduce survival of HEK293 cell line, which did not express CD146 (Supplementary Figures 4C–E), confirming that inhibition was not due to a nonspecific cytotoxic effect. Furthermore, anti-CD146 antibody significantly increased the number of apoptotic cells (Figure 5b and Supplementary Figure 5B), but had no effect on cell proliferation (Figure 5c and Supplementary Figure 5C).

To investigate possible effectors involved CD146-associated apoptosis in MRT, we assessed the activities of Akt, p38 MAPK and Erk, all of which are as downstream targets of CD146.[28–30] Blocking of CD146, either by shRNA knockdown or treatment with an anti-CD146 polyclonal antibody, reduced the phosphorylation of Akt,
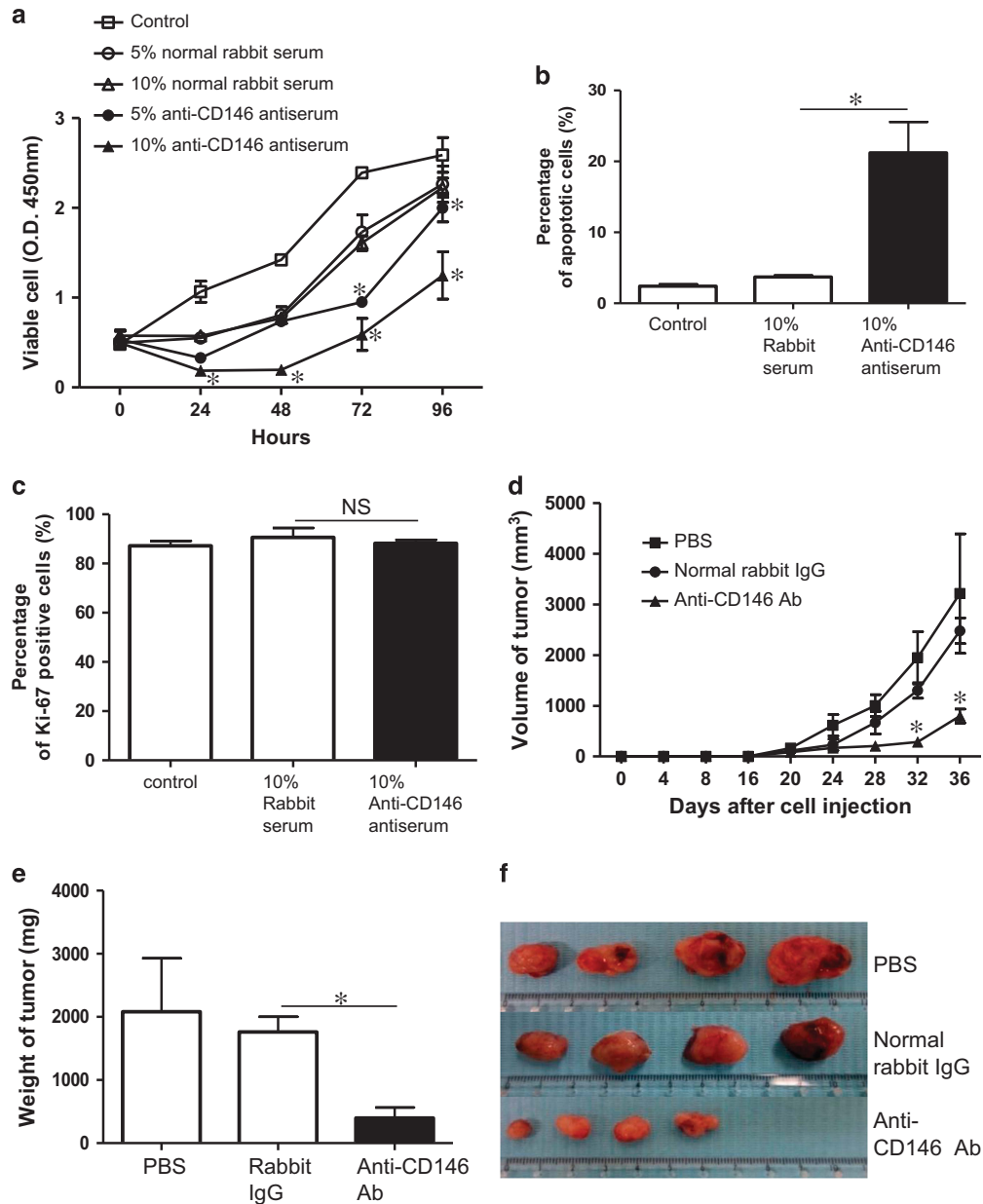
Figure 5. Antitumor activity of anti-CD146 polyclonal antibody against KP-MRT-NS cells. (**a**) WST-8 assays after treatment with normal rabbit serum (5%; open circles, 10%; open triangles), anti-CD146 antiserum (5%; closed circles, 10%; closed triangles), and control culture medium (open squares). P-values were calculated by comparing viable cells at the same serum concentrations. OD, optical density. (**b**) Apoptosis assays after anti-CD146 antiserum treatment. (**c**) Proliferation assays after anti-CD146 antiserum treatment. (**d**) *In vivo* antitumor effects of purified anti-CD146 antibody (Ab) (triangles), normal rabbit IgG (circles), and phosphate-buffered saline (squares) on the volume of tumor cell xenograft tumors in NOG mice. (**e**) Effect on tumor weights. (**f**) Macroscopic appearance of tumor tissues. Error bars indicate s.d. Results shown are representatives of three independent experiments *in vitro* and four independent experiments *in vivo* (*$P < 0.05$). NS, not significant.

but not p38 MAPK or Erk (Supplementary Figures 6A and B). As mammalian target of rapamycin (mTOR) is a vital component of Akt signaling pathway,[31,32] we next examined the effect of mTOR inhibitors. Two highly specific mTOR inhibitors, rapamycin and Ku-0063794, also suppressed survival of KP-MRT-NS cells via induction of apoptosis (Supplementary Figures 7A–D).

Next, to determine whether CD146 expression enhance tumorigenic potential in MRT, we overexpressed CD146 in KP-MRT-YM cells (Supplementary Figure 8A). CD146 overexpression increased sphere-forming capacity and survival of KP-MRT-YM cells (Supplementary Figures 8B and C). Furthermore, overexpression of CD146 significantly decreased apoptosis via

downregulation of Akt phosphorylation without any effect on cell proliferation (Supplementary Figures 8D–F). Similarly, CD146 overexpression in HEK293 cells also increased cell survival by reducing apoptosis (Supplementary Figures 9A–D). Taken together, these data demonstrate that blocking of CD146 suppressed survival of MRT cells by inactivating Akt signaling, thereby inducing apoptosis.

Targeting CD146 inhibited tumor growth of MRT xenografts *in vivo*
We speculated that these findings described above could provide the basis for a novel immunotherapy for MRT. To test this idea, we

investigated the *in vivo* antitumor effect of purified anti-CD146 polyclonal antibody in KP-MRT-NS and MP-MRT-AN cells, which exhibited higher tumorigenicity *in vivo*. Approximately 1 month after anti-CD146 antibody treatment was administered intraperitoneally in NOG mice, both volume and weight of tumors markedly decreased (Figures 5d–f and Supplementary Figures 5D–F). A sustained *in vivo* antitumor effect was observed up to 68 days after transplantation without any obvious adverse effects (Supplementary Figures 10A and B). In addition, immunostaining for single-stranded DNA revealed that apoptotic cells were more abundant in mice treated with purified anti-CD146 antibody than in control mice (Supplementary Figure 11A). Significant inhibition of tumor growth was also observed when CD146 was knocked down (Supplementary Figures 12A–C), supporting the idea that CD146-related mechanisms have important roles in *in vivo* tumor formation.

Previous reports showed that treatment with anti-CD146 antibody inhibits tumor growth or metastasis of various malignancies by disrupting the formation of new intratumoral vessels.[24,33] To confirm this possibility, we immunohistochemically evaluated the vascularity of xenografts using anti-CD31 antibody. However, we observed no difference in microvessel density between mice treated with anti-CD146 antibody and those treated with normal rabbit IgG (Supplementary Figures 11B and C). Collectively, these results show that our anti-CD146 antibody inhibited tumor growth by inducing apoptosis *in vivo*, but not by disrupting the new intratumoral vessels.

Correlation of CD146 expression with clinical outcome of MRT
Finally, we analyzed the association between CD146 expression and the clinical outcomes of 11 cases (13 samples) in our hospitals (Table 2). Five of the 11 cases were CD146+ at the time of the initial diagnosis, and one negative case (patient #6) turned positive at relapse. Five of six CD146+ samples exhibited a focal staining pattern, whereas only one sample (patient #11) exhibited diffuse staining (Supplementary Figure 13). To assess the association between CD146 expression and chemoresistance, we then evaluated the best response to chemotherapy in nine patients (four CD146+ and five CD146−) whose tumor was not completely removed before chemotherapy. Three of the five CD146− cases had a good (complete or partial) response to chemotherapy, whereas only one of the four CD146+ cases had a good response. Other baseline characteristics did not differ significantly between CD146+ and CD146− cases. Three out of

the five CD146− cases survived long term, whereas all six CD146+ cases died within 2 years after initial diagnosis. Thus, expression of CD146 may be associated with poor outcome in patients with MRT.

DISCUSSION

Global gene expression analysis showed that genes involved in neural and/or neural crest development are markedly downregulated in MRT cells, leading to one hypothesis that MRT develops in progenitor cells during neuroectodermal lineage specification.[17] From extensive expression screening using flow cytometric analysis, as well as *in vitro* and *in vivo* studies, we demonstrated that the expression of CD146 defines a distinct subpopulation with high tumorigenic potential in MRT. Purified CD146+ cells could be passaged by serial transplantation in immunodeficient NOG mice, consistent with one of the criteria for TICs.[34] More importantly, CD146+ cells were present in primary MRT tumors and exhibited exclusive *in vivo* tumorigenic potential. More CD146+ cells were observed in cell lines than primary tumors, possibly because TICs may be enriched during selective passages during the establishment of cell lines. Previous reports suggested that CD133+ cells exhibit the characteristics of TICs in MRT.[19,20] However, as CD133+ cells are hardly detected in some MRT cell lines and primary samples, and had inferior sphereforming potential than CD146+ cells in two cell lines, the significance of CD133 in MRT seems to be limited to a few cells that express this protein, as also reported in Ewing sarcoma.[35]

CD146− MRT cells were morphologically indistinguishable from CD146+ cells, and no markers are currently available for differentiated MRT cells. However, our tumor xenograft data demonstrated that CD146+ cells regenerate 'differentiated' CD146− cells that have lost tumorigenicity *in vivo*, strongly suggesting that CD146+ MRT cells have the potential to differentiate, the other criterion for TICs.[34] After serial transplantation of three MRT cell lines, the engrafted tumors consisted predominantly of CD146+ cells. However, purified CD146+ cells from the third transplantation of the three cell lines could produce both CD146+ and CD146− cells *in vitro* (data not shown), suggesting that microenvironment or the xenogenic immune response may favor selective proliferation of human TICs in highly immunodeficient mice.[36]

This study also raised the possibility that CD146 represents a specific therapeutic target for treatment of MRT. As previously reported,[28,37] treatment with anti-CD146 polyclonal antibody or

Table 2. Clinical characteristics, outcome and the CD146 staining pattern in 11 patients with MRT

Patient number	Primary or recurrent tumor	Age at Dx (months)	Tumor site	Meta stasis	CD146 status	Treatment	Best response to chemotherapy	Survival (months)	Outcome
#1	Primary	5	Retroperitoneum	(+)	Pos	C	PD	2	DOD
#2	Primary	72	Cubital fossa	(−)	Neg	S, C	CR	36+	Alive, NED
#3	Primary	19	Cerebellum (ATRT)	(−)	Neg	S, C, R	PR	20	DOD
#4	Primary	10	Basal nuclei (ATRT)	(+)	Pos	S, C, R	PD	5	DOD
#5	Primary	20	Cerebellum (ATRT)	(−)	Pos	None	NA	1	TRM
#6	Primary	2	Kidney (MRTK)	(+)	Neg	S, C, R	PD	11	DOD
	Recurrent	5	Retroperitoneum		Pos				
#7	Primary	At birth	Extracranial head and neck	(−)	Pos	C, R	PD	16	DOD
#8	Primary	3	Chest wall	(−)	Neg	S, C, R	NA	149+	Alive, NED
#9	Primary	2	Kidney (MRTK)	(+)	Neg	S, C	PD	9	DOD
	Recurrent	4	Lung		Neg				
#10	Primary	11	Pelvis	(−)	Neg	C, R	CR	77+	Alive, NED
#11	Primary	7	Neck	(+)	Pos	C, R	PR	10	DOD

Abbreviations: ATRT, atypical teratoid rhabdoid tumor; C, chemotherapy; CR, complete response; DOD, died of disease; DX, diagnosis; MRT, malignant rhabdoid tumor; MRTK, malignant rhabdoid tumor of the kidney; NA, not available; NED, no evidence of disease; Neg, negative; PD, progressive disease; Pos, positive; PR, partial response; R, radiotherapy; S, surgery; TRM, treatment-related mortality. INI1 staining was negative in all tumor specimens.

shRNA knockdown of CD146 directly inhibited tumor growth of MRT cells by inducing apoptosis partially via inactivating Akt, without suppressing microvascular density in xenografts. Besides, other reports demonstrated that anti-CD146 neutralizing antibody exerts antitumor effects against malignancies, including melanoma, osteosarcoma and pancreatic carcinoma, by inhibiting the formation of newly intratumoral vessels.[24,33,38] Thus, CD146 may be involved in different cancer-related pathways for various types of malignancies. Another possible explanation for this discrepancy is that the binding sites of our antibody to tumor vessels may be different from those of the anti-CD146 neutralizing antibody; CD146 may adopt different structures under various conditions, thereby changing the epitopes recognized by anti-CD146 antibody.[39] Alternatively, various factors involved in the neovascularization process, such as CD146-negative adipose-derived stem cells and angiogenic factors (vascular endothelial growth factor, hepatocyte growth factor, basic fibroblast growth factor and stromal cell derived factor-1),[40,41] may attenuate anti-angiogenic effect by blocking CD146-related mechanisms.

In this study, we found that anti-CD146 polyclonal antibody exerted an antitumor effect against MRT in vitro and in NOG mice, suggesting that the antibody inhibits survival of MRT cells by inducing apoptosis without antibody-dependent cell-mediated cytotoxicity or complement-dependent cytotoxicity.[42–44] To determine the distinct roles of complement-dependent cytotoxicity or antibody-dependent cell-mediated cytotoxicity in association with anti-CD146 antibody, it will be necessary to perform further investigations under more suitable experimental conditions.[43]

In many tumors, various biomarkers exist that allow identification of patients with poor prognosis or monitoring of disease status during therapy.[45] Some clinical factors, such as age of onset and therapy regimen, affect clinical outcomes of MRTK and ATRT;[46,47] however, the pathologic prognostic factors in these diseases remain unknown. Although it is difficult to draw a firm conclusion because of the limited sample size of this study, our results also suggest the utility of CD146 as a potent biomarker of MRT, as previously reported in melanoma, breast cancer, clear-cell renal cell carcinoma and lung adenocarcinoma.[22] It would be desirable to validate the utility of CD146 as a biomarker for risk stratification of MRT in a large prospective study.

MATERIALS AND METHODS

Cell lines, tumor samples and animals
The human MRT cell lines MP-MRT-AN, KP-MRT-NS, KP-MRT-RY and KP-MRT-YM were established as previously reported.[48–51] The HEK293 cell line was purchased from JCRB Cell Bank (Osaka, Japan; JCRB9068, FL Graham). The MRT cell lines were cultured in RPMI-1640 medium containing penicillin, streptomycin, L-glutamine, and 10% heat-inactivated fetal bovine serum. HEK293 cell lines were cultured in Dulbecco's modified Eagle's medium containing penicillin, streptomycin, L-glutamine and 10% fetal bovine serum. These cell lines were regularly tested to ensure that they are mycoplasma free. All culture incubations were performed in a humidified 37 °C, 5% CO$_2$ incubator. Diagnosis of MRT was made according to histological findings and immunostaining for INI1. Tumor samples were collected from patients with MRT whose parents provided written informed consent under the guidelines of the Kyoto University Graduate School and Faculty of Medicine Ethics Committee. All experiments involving mice were approved by the Institute of Laboratory Animals at the Graduate School of Medicine, Kyoto University. NOD/Shi-scid/IL-2 R ^{null} (NOG) mice were obtained from the Central Institute of Experimental Animals (Kawasaki, Japan) and used at 8–12 weeks of age. Mice were housed in sterile enclosures under specific pathogen-free conditions. These mice were randomly divided into each group before experiment and were anesthetized with isoflurane for all procedures and killed at the end of each experiment.

Flow cytometric analysis and cell sorting
The following primary antibodies were used: anti-CD9–fluorescein isothiocyanate (FITC), anti-CD34–FITC, anti-CD45–FITC, anti-CD56–phycoerythrin (PE), anti-CD73–PE, anti-CD81–PE, anti-CD166–PE, anti-CD106–allophyco-cyanin (APC), anti-CD117–APC and anti-CD271–Alexa Fluor 647 (BD Pharmingen, San Diego, CA, USA); anti-CD29–FITC (eBioscience, San Diego, CA, USA), anti-CD31–FITC, anti-CD105–FITC and anti-Ki-67–APC (BioLegend, San Diego, CA, USA), anti-CD146–PE, anti-CD146–APC, anti-CD133–PE and anti-CD133–APC (Miltenyi Biotec, Bergisch Gladbach, Germany); and anti-TRA-1-85–APC (R&D Systems, Minneapolis, MN, USA). All antibodies were directed against human proteins. Tumor samples and xenografted tumors were co-stained with anti-human CD45, CD34 and CD31 antibodies to identify (and exclude) hematopoietic and endothelial cells, whereas anti-TRA-1-85 antibody was used to distinguish human cells from mouse tissue. Non-viable cells were excluded from the analysis by co-staining with Cytox Blue dead-cell stain (Molecular Probes, Eugene, OR, USA). Flow cytometric analyses were performed on a FACSVerse instrument equipped with the FACSuite software (BD Biosciences, San Jose, CA, USA), and cell sorting was performed on a FACSAriaII equipped with the FACSDiva software (BD Biosciences). Cell sorting was conducted after cells were stained with PE-conjugated anti-CD146 antibody, and flow cytometric reanalysis of the sorted cells demonstrated that their purity ranged from 95 to 99%.

Sphere formation assay
Single cells were plated at 2500 cells/ml on low-attachment EZ-BindShut plates (IWAKI, Chiba, Japan) and cultured in serum-free Dulbecco's modified Eagle's medium:F12 medium (Invitrogen, Carlsbad, CA, USA) supplemented with 20 ng/ml human recombinant EGF (Sigma-Aldrich, St Louis, MO, USA), 20 ng/ml human recombinant basic fibroblast growth factor (Invitrogen), and B27 supplement (1:50; Invitrogen). Ten days later, spheres 50 μm or larger in diameter were counted on an Olympus IX70 inverted microscope (Olympus, Tokyo, Japan) equipped with AxioVison software (Carl Zeiss, Jena, Germany).

Invasion assay
Invasion assays were conducted in BioCoat Matrigel Invasion Chambers (24-well, 8-μm pore, BD Biosciences). Control insert chambers (24-well, 8-μm pore, BD Biosciences) were used for migration assays. In brief, cells (2.5×10^4) suspended in RPMI-1640 were added to the top chamber, and RPMI-1640 supplemented with 10% fetal bovine serum was added to the bottom chamber as a chemoattractant. After a 24-h incubation at 37 °C, cells invading through the Matrigel or control membrane were fixed with 4% paraformaldehyde (Wako, Osaka, Japan) and stained with Diff-Quik stain (Sysmex, Kobe, Japan). The number of cells in each membrane was counted on an Olympus BX50 microscope (Olympus) equipped with the cellSens software (Olympus). The results were calculated using the following formula: %invasion = (number of invading cells)/(number of migrating cells) × 100.

RNA extraction, complementary DNA synthesis, and real-time qRT–PCR
Total RNA was isolated using the RNeasy Mini kit (Qiagen, Valencia, CA, USA). Complementary DNA was synthesized using the Omniscript RT Kit (Qiagen), and then subjected to qRT–PCR analysis. Real-time monitoring of the following genes was performed using TaqMan probes (Life Technologies, Carlsbad, CA, USA) on ABI Prism 7900 system (Applied Biosystems, Foster City, CA, USA): melanoma cell adhesion molecule (MCAM) (MCAM, Hs00174838_m1) and ACTB (ACTB, Hs01060665_g1).

Immunohistochemistry and immunofluorescence
Tissue samples were stored in 4% paraformaldehyde for immunohistochemical analysis. Specimens were embedded in paraffin, and sections (5 μm thick) were subjected to hematoxylin/eosin staining to confirm the pathological features. Next, sections were processed by heat-induced antigen retrieval in citrate buffer, pH 6.0 (Sigma-Aldrich) before they were stained with anti-CD146 (Abcam, Cambridge, MN, USA), anti-CD31 (Abcam), anti-single-stranded DNA (IBL,Takasaki, Japan) and anti-INI1 (Santa Cruz Biotechnology, Dallas, TX, USA) antibodies. Subsequent staining was carried using the Vectastain Elite kit and ImmPACT DAB (Vector Laboratories, Burlingame, CA, USA). CD146 was scored positive if tumor cells with membranous staining were present. The number of blood

vessels per tumor in each group was quantified in at least five random areas per section. Images were taken on an Olympus BX50 microscope equipped with the cellSens software. For immunofluorescence staining of MRT cells to verify the specificity of the antiserum, cells were fixed in 4% paraformaldehyde, and diluted serum (1:10) was used as the first antibody. The secondary antibody was Cy3 donkey anti-rabbit IgG (Jackson ImmunoResearch Laboratories, West Grove, PA, USA). Nuclear DNA was counterstained with Hoechst 33342 (Molecular Probes), and cells were observed on an Olympus IX70 inverted microscope (Olympus) equipped with the AxioVison software (Carl Zeiss).

Western blotting

M-PER mammalian protein extraction reagent (Pierce, Rockford, IL, USA) was used to prepare cell lysates. Equal amounts of total protein were resolved on sodium dodecyl sulfate–polyacrylamide gel electrophoresis, transferred onto Immobilon polyvinylidene difluoride membrane (Millipore, Billerica, MA, USA), and probed with rabbit anti-CD146 (Abcam), rabbit anti-Akt, phospho-Akt (Ser 473), p38 MAPK, phospho-p38 MAPK (Thr180/Tyr182), Erk1/2, phospho-Erk1/2 (Thr202/Tyr204) (Cell Signaling Technology, Danvers, MA, USA), mouse anti-HaloTag (Promega, Madison, WI, USA) and mouse anti-β-actin (Santa Cruz Biotechnology). The antibody signal was detected using an enhanced chemiluminescence system (Amersham ECL Western Blotting Detection Reagents, GE Healthcare Life Science, Uppsala, Sweeden). To verify the specificity of antiserum, diluted antiserum (1:4000) was used as the antibody to detect CD146. Next, the membranes were incubated with horseradish peroxidase-conjugated secondary antibodies (Santa Cruz Biotechnology). The antibody signal was detected using Amersham ECL Western Blotting Detection Reagents (GE Healthcare Life Science).

Transfection with CD146 shRNA

Two distinct shRNA plasmids targeting human CD146 mRNA (TG311550A, shRNA#1; TG311550D, shRNA#2) and a scrambled control shRNA plasmid (TR30013, scrambled shRNA) were purchased from OriGene (Rockville, MD, USA). All plasmids expressed green fluorescent protein (GFP) as a marker for transfection. KP-MRT-NS cells were transfected with FuGENE HD (Roche Applied Science, Indianapolis, IN, USA). For selection of stable knockdowns, cells were cultured in normal medium containing puromycin, and GFP$^+$ cells were isolated by cell sorting on a FACSAriaII. Knockdown efficiency was determined by qRT–PCR and western blotting.

Transfection of CD146 complementary DNA

CD146 expression vector was constructed from Flexi clone FXC10514 (Kazusa DNA Research Institute, Chiba, Japan) and the pFN28A Halotag CMV-neo Flexi vector (Promega) using the Flexi cloning system. KP-MRT-YM and HEK293 cells were transfected with FuGENE HD and cultured in normal medium containing G418 (Sigma-Aldrich Japan, Tokyo, Japan) for selection of stable cell lines (YM/CD146 and HEK/CD146 cells). Controls for CD146 expression were cell lines transfected with pFN28A control vector (YM/pFN28A and HEK/pFN28A cells). Overexpression of CD146 was evaluated by western blotting.

Generation of rabbit anti-CD146 polyclonal antibody

Anti-peptide serum against the extracellular part of CD146 was generated by injecting immunizing peptides into rabbits (Sigma-Aldrich Japan). The immunizing peptides consisted of 17 amino acids from the extracellular domain. Specificity of the antibody was confirmed by western blotting and immunofluorescence using the CD146-expressing KP-MRT-NS cell line.

Cell viability measurements

Cells were plated in normal growth medium in 96-well cell culture plate (2000 cells per well). After 6 h, the medium was exchanged. To determine the effect of antiserum, inactivated antiserum against CD146 or normal rabbit serum (Life Technologies) was added to culture medium for adjusting to a final concentration of 5% or 10% (v/v). To determine the effect of mTOR inhibitors, various concentrations of rapamycin (Wako) and Ku-0063794 (Wako) were added to culture medium. Cell viability was measured every 24 h for 4 days by WST-8 assay using the Cell Counting Kit-8 (Dojin, Kumamoto, Japan) on a Benchmark Microplate Reader (Bio-Rad, Hercules, CA, USA).

Apoptosis and proliferation assays

Six hours after cells were plated on the dish, treatment was initiated by adding inactivated antiserum against CD146 or normal rabbit serum to the culture medium for adjusting to a final concentration of 10% (v/v). To determine the effect of mTOR inhibitors, rapamycin (1 nM) and Ku-0063794 (1000 nM) were added to culture medium. Sixteen hours later, apoptosis was evaluated by Annexin V/7-aminoactinomycin D (7-AAD) staining (BD Biosciences) and cell proliferation was evaluated by Ki-67 staining. Apoptosis and proliferation of shRNA-treated cells was evaluated 48 h after plating. Apoptotic cells were defined as Annexin V$^+$/7-AAD$^-$ cells.

Sorted cell implantation into NOG mice and serial transplantation

MRT cell lines were treated with 0.05% trypsin/EDTA (Life Technologies), and sorted cells were resuspended in serum-free α-minimum essential medium for experiments. For fresh tumor samples, specimens were mechanically dissociated and filtered through a 70-μm mesh to obtain single cells, and the sorted cells were resuspended in serum-free α-minimum essential medium supplemented with 50% BD Matrigel Matrix Growth Factor Reduced mixture (BD Biosciences). CD146$^+$ cells or CD146$^-$ cells that did not stain with CD34/45/31 on flow cytometric analysis were injected. Subcutaneous injections into the flanks of NOG mice were performed using 27-gauge needles. Tumor formation was serially evaluated until 12 weeks after implantation, when all mice were killed and subjected to further experiments. In some experiments, serial transplantations were performed as described for fresh clinical tissue specimens.

In vivo antitumor activity of polyclonal antibody and shRNA silencing of CD146

KP-MRT-NS- or MP-MRT-AN-bearing mice were treated with rabbit normal IgG or anti-CD146 polyclonal antibody purified using a peptide column. One week after injection of 1.0×10^5 tumor cells into the flanks of NOG mice, rabbit normal IgG or anti-CD146 antibody at a dose of 400 μg/kg or phosphate-buffered saline was administered intraperitoneally, twice a week, until mice were killed. Regarding the silencing of CD146, 1.0×10^5 shRNA-treated cells were injected subcutaneously into the flanks of NOG mice. Tumor size was measured every 4 days, and tumor volume was determined according to the following equation: tumor size = width$^2 \times$ length $\times (\pi/6)$. The investigator was blinded to the group allocation during the experiment. For immunohistological analysis, tumors were removed and subjected to further experiments at the end of experiments (day 36 for KP-MRT-NS; day 44 for MR-MRT-AN and shRNA-treated cells). For long-term analysis, mice were treated under the same conditions until day 68.

Efficacy assessment of chemotherapy

For all patients, radiographic changes (complete response, partial response, stable disease and progressive disease) were evaluated by investigators using the (Response Evaluation Criteria in Solid Tumors (RECIST) version 1.1 (The European Organisation for Research and Treatment of Cancer, Brussels, Belgium).

Statistical analysis

Data are expressed as means ± s.d. Differences in mean values between groups were analyzed by Student's t-test. Multiple comparisons used one-way or two-way analysis of variance with the post hoc Bonferroni multiple comparison test. Estimates of variation within each group were performed and variances were similar between all the statistically compared groups. All statistical analyses were performed using the GraphPad Prism software (version 5; GraphPad Software, San Diego, CA, USA). For animal studies, sample size was estimated to be at least four mice per group to ensure power with statistical confidence. Limiting dilution analyses were carried out using extreme limiting dilution analysis as described previously.[52] TIC frequencies were compared using the likelihood rate test. Values of $P < 0.05$ were considered statistically significant.

CONFLICT OF INTEREST

The authors declare no conflict of interest.

REFERENCES
1 Sultan I, Qaddoumi I, Rodriguez-Galindo C, Nassan AA, Ghandour K, Al-Hussaini M. Age, stage, and radiotherapy, but not primary tumor site, affects the outcome of patients with malignant rhabdoid tumors. *Pediatr Blood Cancer* 2010; **54**: 35–40.

2 Ginn KF, Gajjar A. Atypical teratoid rhabdoid tumor: current therapy and future directions. *Front Oncol* 2012; **2**: 114.

3 Weeks DA, Beckwith JB, Mierau GW, Luckey DW. Rhabdoid tumor of kidney. A report of 111 cases from the National Wilms' Tumor Study Pathology Center. *Am J Surg Pathol* 1989; **13**: 439–458.

4 Ho DM, Hsu CY, Wong TT, Ting LT, Chiang H. Atypical teratoid/rhabdoid tumor of the central nervous system: a comparative study with primitive neuroectodermal tumor/medulloblastoma. *Acta Neuropathol* 2000; **99**: 482–488.

5 Hilden JM, Meerbaum S, Burger P, Finlay J, Janss A, Scheithauer BW et al. Central nervous system atypical teratoid/rhabdoid tumor: results of therapy in children enrolled in a registry. *J Clin Oncol* 2004; **22**: 2877–2884.

6 Versteege I, Sevenet N, Lange J, Rousseau-Merck MF, Ambros P, Handgretinger R et al. Truncating mutations of hSNF5/INI1 in aggressive paediatric cancer. *Nature* 1998; **394**: 203–206.

7 Biegel JA, Zhou JY, Rorke LB, Stenstrom C, Wainwright LM, Fogelgren B. Germ-line and acquired mutations of INI1 in atypical teratoid and rhabdoid tumors. *Cancer Res* 1999; **59**: 74–79.

8 van den Heuvel-Eibrink MM, van Tinteren H, Rehorst H, Coulombe A, Patte C, de Camargo B et al. Malignant rhabdoid tumours of the kidney (MRTKs), registered on recent SIOP protocols from 1993 to 2005: a report of the SIOP renal tumour study group. *Pediatr Blood Cancer* 2011; **56**: 733–737.

9 Magee JA, Piskounova E, Morrison SJ. Cancer stem cells: impact, heterogeneity, and uncertainty. *Cancer Cell* 2012; **21**: 283–296.

10 Visvader JE, Lindeman GJ. Cancer stem cells: current status and evolving complexities. *Cell Stem Cell* 2012; **10**: 717–728.

11 Clevers H. The cancer stem cell: premises, promises and challenges. *Nat Med* 2011; **17**: 313–319.

12 Bonnet D, Dick JE. Human acute myeloid leukemia is organized as a hierarchy that originates from a primitive hematopoietic cell. *Nat Med* 1997; **3**: 730–737.

13 Al-Hajj M, Wicha MS, Benito-Hernandez A, Morrison SJ, Clarke MF. Prospective identification of tumorigenic breast cancer cells. *Proc Natl Acad Sci USA* 2003; **100**: 3983–3988.

14 Singh SK, Hawkins C, Clarke ID, Squire JA, Bayani J, Hide T et al. Identification of human brain tumour initiating cells. *Nature* 2004; **432**: 396–401.

15 Zhou BB, Zhang H, Damelin M, Geles KG, Grindley JC, Dirks PB. Tumour-initiating cells: challenges and opportunities for anticancer drug discovery. *Nat Rev Drug Disc* 2009; **8**: 806–823.

16 Okuno K, Ohta S, Kato H, Taga T, Sugita K, Takeuchi Y. Expression of neural stem cell markers in malignant rhabdoid tumor cell lines. *Oncol Rep* 2010; **23**: 485–492.

17 Gadd S, Sredni ST, Huang CC, Perlman EJ. Rhabdoid tumor: gene expression clues to pathogenesis and potential therapeutic targets. *Lab Invest* 2010; **90**: 724–738.

18 Parham DM, Weeks DA, Beckwith JB. The clinicopathologic spectrum of putative extrarenal rhabdoid tumors. An analysis of 42 cases studied with immunohistochemistry or electron microscopy. *Am J Surg Pathol* 1994; **18**: 1010–1029.

19 Chiou SH, Kao CL, Chen YW, Chien CS, Hung SC, Lo JF et al. Identification of CD133-positive radioresistant cells in atypical teratoid/rhabdoid tumor. *PloS One* 2008; **3**: e2090.

20 Yanagisawa S, Kadouchi I, Yokomori K, Hirose M, Hakozaki M, Hojo H et al. Identification and metastatic potential of tumor-initiating cells in malignant rhabdoid tumor of the kidney. *Clin Cancer Res* 2009; **15**: 3014–3022.

21 Shih IM. The role of CD146 (Mel-CAM) in biology and pathology. *J Pathol* 1999; **189**: 4–11.

22 Wang Z, Yan X. CD146, a multi-functional molecule beyond adhesion. *Cancer Lett* 2013; **330**: 150–162.

23 Pujades C, Guez-Guez B, Dunon D. Melanoma cell adhesion molecule (MCAM) expression in the myogenic lineage during early chick embryonic development. *Int J Dev Biol* 2002; **46**: 263–266.

24 Mills L, Tellez C, Huang S, Baker C, McCarty M, Green L et al. Fully human antibodies to MCAM/MUC18 inhibit tumor growth and metastasis of human melanoma. *Cancer Res* 2002; **62**: 5106–5114.

25 Zhong Y, Guan K, Guo S, Zhou C, Wang D, Ma W et al. Spheres derived from the human SK-RC-42 renal cell carcinoma cell line are enriched in cancer stem cells. *Cancer Lett* 2010; **299**: 150–160.

26 Chen D, Bhat-Nakshatri P, Goswami C, Badve S, Nakshatri H. ANTXR1, a stem cell-enriched functional biomarker, connects collagen signaling to cancer stem-like cells and metastasis in breast cancer. *Cancer Res* 2013; **73**: 5821–5833.

27 Meacham CE, Morrison SJ. Tumour heterogeneity and cancer cell plasticity. *Nature* 2013; **501**: 328–337.

28 Li G, Kalabis J, Xu X, Meier F, Oka M, Bogenrieder T et al. Reciprocal regulation of MelCAM and AKT in human melanoma. *Oncogene* 2003; **22**: 6891–6899.

29 Jiang T, Zhuang J, Duan H, Luo Y, Zeng Q, Fan K et al. CD146 is a coreceptor for VEGFR-2 in tumor angiogenesis. *Blood* 2012; **120**: 2330–2339.

30 Tu T, Zhang C, Yan H, Luo Y, Kong R, Wen P et al. CD146 acts as a novel receptor for netrin-1 in promoting angiogenesis and vascular development. *Cell Res* 2015; **25**: 275–287.

31 Laplante M, Sabatini DM. mTOR signaling in growth control and disease. *Cell* 2012; **149**: 274–293.

32 Zoncu R, Efeyan A, Sabatini DM. mTOR: from growth signal integration to cancer, diabetes and ageing. *Nat Rev Mol Cell Biol* 2011; **12**: 21–35.

33 Yan X, Lin Y, Yang D, Shen Y, Yuan M, Zhang Z et al. A novel anti-CD146 monoclonal antibody, AA98, inhibits angiogenesis and tumor growth. *Blood* 2003; **102**: 184–191.

34 Clarke MF, Dick JE, Dirks PB, Eaves CJ, Jamieson CH, Jones DL et al. Cancer stem cells--perspectives on current status and future directions: AACR Workshop on cancer stem cells. *Cancer Res* 2006; **66**: 9339–9344.

35 Jiang X, Gwye Y, Russell D, Cao C, Douglas D, Hung L et al. CD133 expression in chemo-resistant Ewing sarcoma cells. *BMC Cancer* 2010; **10**: 116.

36 Stewart JM, Shaw PA, Gedye C, Bernardini MQ, Neel BG, Ailles LE. Phenotypic heterogeneity and instability of human ovarian tumor-initiating cells. *Proc Natl Acad Sci USA* 2011; **108**: 6468–6473.

37 Jouve N, Despoix N, Espeli M, Gauthier L, Cypowyj S, Fallague K et al. The involvement of CD146 and its novel ligand Galectin-1 in apoptotic regulation of endothelial cells. *J Biol Chem* 2013; **288**: 2571–2579.

38 McGary EC, Heimberger A, Mills L, Weber K, Thomas GW, Shtivelband M et al. A fully human antimelanoma cellular adhesion molecule/MUC18 antibody inhibits spontaneous pulmonary metastasis of osteosarcoma cells in vivo. *Clin Cancer Res* 2003; **9**: 6560–6566.

39 Zhang Y, Zheng C, Zhang J, Yang D, Feng J, Lu D et al. Generation and characterization of a panel of monoclonal antibodies against distinct epitopes of human CD146. *Hybridoma* 2008; **27**: 345–352.

40 Rehman J, Traktuev D, Li J, Merfeld-Clauss S, Temm-Grove CJ, Bovenkerk JE et al. Secretion of angiogenic and antiapoptotic factors by human adipose stromal cells. *Circulation* 2004; **109**: 1292–1298.

41 Yoshimura K, Shigeura T, Matsumoto D, Sato T, Takaki Y, Aiba-Kojima E et al. Characterization of freshly isolated and cultured cells derived from the fatty and fluid portions of liposuction aspirates. *J Cell Physiol* 2006; **208**: 64–76.

42 Ito M, Hiramatsu H, Kobayashi K, Suzue K, Kawahata M, Hioki K et al. NOD/SCID/gamma(c)(null) mouse: an excellent recipient mouse model for engraftment of human cells. *Blood* 2002; **100**: 3175–3182.

43 Ito A, Ishida T, Utsunomiya A, Sato F, Mori F, Yano H et al. Defucosylated anti-CCR4 monoclonal antibody exerts potent ADCC against primary ATLL cells mediated by autologous human immune cells in NOD/Shi-scid, IL-2 R gamma(null) mice in vivo. *J Immunol* 2009; **183**: 4782–4791.

44 Shiokawa M, Takahashi T, Murakami A, Kita S, Ito M, Sugamura K et al. In vivo assay of human NK-dependent ADCC using NOD/SCID/gammac(null) (NOG) mice. *Biochem Biophys Res Commun* 2010; **399**: 733–737.

45 Sawyers CL. The cancer biomarker problem. *Nature* 2008; **452**: 548–552.

46 Tomlinson GE, Breslow NE, Dome J, Guthrie KA, Norkool P, Li S et al. Rhabdoid tumor of the kidney in the National Wilms' Tumor Study: age at diagnosis as a prognostic factor. *J Clin Oncol* 2005; **23**: 7641–7645.

47 Tekautz TM, Fuller CE, Blaney S, Fouladi M, Broniscer A, Merchant TE et al. Atypical teratoid/rhabdoid tumors (ATRT): improved survival in children 3 years of age and older with radiation therapy and high-dose alkylator-based chemotherapy. *J Clin Oncol* 2005; **23**: 1491–1499.

48 Sugimoto T, Hosoi H, Horii Y, Ishida H, Mine H, Takahashi K et al. Malignant rhabdoid-tumor cell line showing neural and smooth-muscle-cell phenotypes. *Int J Cancer* 1999; **82**: 678–686.

49 Kuroda H, Moritake H, Sawada K, Kuwahara Y, Imoto I, Inazawa J et al. Establishment of a cell line from a malignant rhabdoid tumor of the liver lacking the

function of two tumor suppressor genes, hSNF5/INI1 and p16. *Cancer Genet Cytogenet* 2005; **158**: 172–179.

50 Katsumi Y, Kuwahara Y, Tamura S, Kikuchi K, Otabe O, Tsuchiya K *et al.* Trastuzumab activates allogeneic or autologous antibody-dependent cellular cytotoxicity against malignant rhabdoid tumor cells and interleukin-2 augments the cytotoxicity. *Clin Cancer Res* 2008; **14**: 1192–1199.

51 Misawa A, Hosoi H, Imoto I, Iehara T, Sugimoto T, Inazawa J. Translocation (1;22) (p36;q11.2) with concurrent del(22)(q11.2) resulted in homozygous deletion of SNF5/INI1 in a newly established cell line derived from extrarenal rhabdoid tumor. *J Human Genet* 2004; **49**: 586–589.

52 O'Brien CA, Kreso A, Jamieson CH. Cancer stem cells and self-renewal. *Clin Cancer Res* 2010; **16**: 3113–3120.

Supplementary Information accompanies this paper on the Oncogene website (http://www.nature.com/onc)